

Symmetry-preserving and gate-efficient quantum circuits for quantum chemistry

Hugh G. A. Burton^{1,*}

¹*Yusuf Hamied Department of Chemistry, University of Cambridge, Lensfield Road, Cambridge, CB2 1EW, U.K.*

(Dated: January 12, 2024)

arXiv:2312.09761v2 [physics.chem-ph] 11 Jan 2024

Abstract

The ability of quantum computers to overcome the exponential memory scaling of many-body problems is expected to transform quantum chemistry. Quantum algorithms require accurate representations of electronic states on a quantum device, but current approximations struggle to combine chemical accuracy and gate-efficiency while preserving physical symmetries, and rely on measurement-intensive adaptive methods that tailor the wave function *ansatz* to each molecule. In this contribution, we present a spin-symmetry-preserving, gate-efficient *ansatz* that provides chemically accurate molecular energies with a well-defined circuit structure. Our approach exploits local qubit connectivity, orbital optimisation, and connections with generalised valence bond theory to maximise the accuracy that is obtained with shallow quantum circuits. Numerical simulations for molecules with weak and strong electron correlation, including benzene, water, and the singlet-triplet gap in tetramethylethane, demonstrate that chemically accurate energies are achieved with as much as 84 % fewer two-qubit gates compared to the current state-of-the-art. These advances pave the way for the next generation of electronic structure approximations for future quantum computing.

Introduction

Solving the electronic Schrödinger equation underpins theoretical predictions of chemistry. Since exact solutions formally scale exponentially with the number of electrons, we currently rely on polynomially-scaling approximations, such as coupled-cluster and density functional theory. However, these methods fail when electronic states cannot be easily approximated, due to strong spin-coupling or competing electronic configurations. Gate-based quantum computation promises to solve these strongly correlated problems by representing electronic states using polynomially scaling quantum resources.⁽¹⁾ For near-term quantum hardware, which is limited to shallow quantum circuits, the most promising approaches optimise a parametrised *ansatz* for the electronic state using algorithms such as the variational quantum eigensolver (VQE).⁽²⁾ However, traditional electronic structure approximations cannot be easily translated into quantum circuits, and no consensus has been reached on the best *ansatz* for practical quantum computation.^(3, 4)

We define a quantum *ansatz* as a parametrised unitary transformation \hat{U} applied to an initial qubit state $|\Phi_0\rangle$, where \hat{U} is composed of building blocks $\hat{U} = \hat{U}_1(\theta_1) \cdots \hat{U}_M(\theta_M)$ that are implemented using quantum gate operations. This *ansatz* should (i) be highly accurate and systematically improvable, (ii) correspond to a shallow quantum circuit, and (iii) satisfy the physical symmetries of the Hamiltonian including the particle number, Pauli antisymmetry, and the $\langle \hat{S}^2 \rangle$ and $\langle \hat{S}_z \rangle$ spin quantum numbers. Generally, \hat{U} is constructed using either hardware-efficient operators, which give shallow circuits but fail to preserve physical symmetries,^(5–8) or fermionic operators that preserve physical symmetries, but require a large number of gate operations.^(3, 9–16) For example, methods based on unitary coupled cluster (UCC) theory expand the exponential of a sum of non-commuting fermionic operators using a Trotter approximation $e^{\hat{A}+\hat{B}} = \lim_{m \rightarrow \infty} (e^{\hat{A}/m} e^{\hat{B}/m})^m$, which is only exact in the infinite limit.^(2, 3, 17) Overcoming this trade-off between gate efficiency and physical symmetries will be essential for chemically meaningful calculations on near-term devices.

A major advance towards gate efficiency using fermionic operators was the disentangled UCC approach, which showed that exact wave functions can be constructed from an infinite product of exponential one- and two-body fermionic operators.⁽¹⁸⁾ However, the accuracy of truncated expansions strongly depends on the choice and ordering of operators.^(17–19) State-of-the-art algorithms overcome this challenge by using an adaptive *ansatz* that is constructed by iteratively adding operators with the largest energy improvement at each step through the ADAPT-VQE

* hgaburton@gmail.com

protocol,(20–24) or by discretely optimising the operator sequence.(25) These approaches have shown that accurate and gate-efficient approximations of electronic states can be identified, while even shallower quantum circuits can be constructed using qubit-excitation-based operators at the expense of broken Pauli antisymmetry.(24, 26) However, this adaptive optimisation has high quantum measurement costs that are likely to preclude simulations on real hardware, and can yield very different circuits with inconsistent hardware noise along a potential energy surface.

In this work, we present the tiled Unitary Product State (tUPS) approximation and show that it can provide high-accuracy, spin-preserving, and gate-efficient quantum circuits. Building on the quantum number preserving (QNP) gate fabric, which combines symmetry-preservation with local qubit connectivity,(27) our approach maximises the accuracy for shallow quantum circuits by incorporating orbital optimisation and an initial qubit state motivated by perfect-pairing valence bond theory. Numerical simulations demonstrate that chemical accuracy (within 1.59 mE_h) can be obtained for potential energy surfaces and spin-state energies in molecules with weak and strong electron correlation, using up to 84 % fewer two-qubit gates compared to state-of-the-art adaptive algorithms. Our results comprehensively show that the fixed UPS *ansatz* can exceed the accuracy and gate efficiency of adaptive optimisation methods, paving the way for the next generation of electronic structure approximations for quantum algorithms.

Results

Tiled unitary product states

Building on disentangled UCC theory,(18) we have recently shown that an arbitrary wave function can be constructed from a product of M unitary fermionic operators as(25)

$$|\Psi(\boldsymbol{\theta})\rangle = \prod_{I=1}^M \exp(\theta_I \hat{\kappa}_{\mu_I}) |\Phi_0\rangle, \quad (1)$$

where $\hat{\kappa}_{\mu_I}$ includes only spin-adapted one-body operators $\hat{\kappa}_{pq}^{(1)}$ or paired two-body operators $\hat{\kappa}_{pq}^{(2)}$ acting between spatial orbitals ϕ_p and ϕ_q , defined as

$$\hat{\kappa}_{pq}^{(1)} = \hat{E}_{pq} - \hat{E}_{qp}, \quad \text{and} \quad \hat{\kappa}_{pq}^{(2)} = \hat{E}_{pq}^2 - \hat{E}_{qp}^2. \quad (2)$$

Here, $\hat{E}_{pq} = \hat{p}^\dagger \hat{q} + \hat{p} \hat{q}^\dagger$ is the singlet excitation operator,(28) \hat{p}^\dagger (\hat{p}) defines the creation operator for a high (low) spin electron in spatial orbital ϕ_p , $|\Phi_0\rangle$ is the initial state, and θ_I are continuous parameters. Each operator may appear multiple times with a different continuous parameter, and the particular sequence of operators is indexed by the discrete variables μ_I . Any state with the same particle number and spin symmetry as $|\Phi_0\rangle$ can be represented for $M \rightarrow \infty$ using a suitable operator sequence and set of continuous variables. Following Ref. (25), we refer to the *ansatz* in Eq. (1) as a Unitary Product State (UPS) to highlight its general mathematical structure.

In practice, we require a truncated UPS with a finite number of operators and a shallow circuit implementation. Building on the QNP gate fabric,(27) we define the tiled Unitary Product State (tUPS) using L layers of fermionic operators that act between sequential spatial orbitals (Fig. 1A) as

$$|\Psi_{\text{tUPS}}\rangle = \prod_{m=1}^L \left(\prod_{p=1}^A \hat{U}_{2p+1,2p}^{(m)} \prod_{p=1}^B \hat{U}_{2p,2p-1}^{(m)} \right) |\Phi_0\rangle, \quad (3)$$

where $A = \frac{N-2}{2}$ or $\frac{N-1}{2}$ and $B = \frac{N}{2}$ or $\frac{N-1}{2}$ for an even or odd number of spatial orbitals N . The

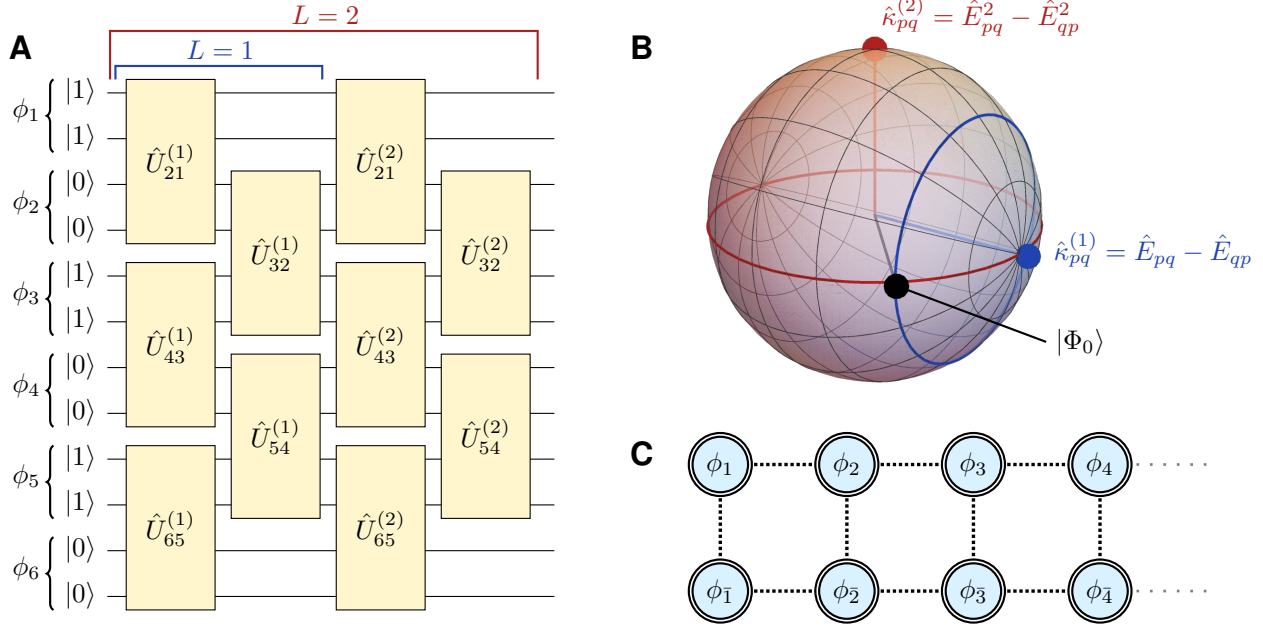


FIG. 1: **(A)** The tUPS *ansatz* employs a tiled gate fabric with L layers containing operators that only couple adjacent spatial orbitals. **(B)** Spin-adapted one-body and paired-two body operators correspond to Givens rotations around orthogonal axes in the singlet subspace where the spatial orbitals ϕ_p and ϕ_q contain a total of one high-spin and one low-spin electron. Arbitrary states within this subspace exist on the surface of a sphere due to normalisation. **(C)** Ordering the qubits such that the high-spin orbitals appear before the low-spin orbitals removes all the Pauli- Z strings from the Jordan–Wigner encoding of $\hat{\kappa}_{pq}^{(1)}$ and $\hat{\kappa}_{pq}^{(2)}$, and a suitable 2D arrangement means that only local connectivity between qubits with the same spatial orbital is required.

operators $\hat{U}_{pq}^{(m)}$ each contain three unique variable parameters for every layer m and are constructed from a paired two-body operator sandwiched between two spin-adapted one-body operators as

$$\hat{U}_{pq}^{(m)} = \exp\left(\theta_{pq,1}^{(m)} \hat{\kappa}_{pq}^{(1)}\right) \exp\left(\theta_{pq,2}^{(m)} \hat{\kappa}_{pq}^{(2)}\right) \exp\left(\theta_{pq,3}^{(m)} \hat{\kappa}_{pq}^{(1)}\right). \quad (4)$$

These operators are not restricted to occupied-virtual orbital pairs, and thus correspond to generalised many-body excitations.⁽⁹⁾ So far, this circuit is almost identical to the QNP approach, but our definition of $\hat{U}_{pq}^{(m)}$ contains two one-body operators rather than just one, giving faster convergence with respect to the number of layers. The accuracy of the tUPS approximation can be increased further by including orbital optimisation and modifying the initial qubit register using connections to the perfect pairing generalised valence bond theory,^(29–33) leading to the orbital-optimised (oo-tUPS) and perfect-pairing (pp-tUPS) variants of the tUPS approximation, respectively (*vide infra*).

Optimal ordering of unitary operations

The properties of $\hat{U}_{pq}^{(m)}$ can be understood by characterising how the exponential unitary operators $\exp(\theta \hat{\kappa}_{pq}^{(1)})$ and $\exp(\theta \hat{\kappa}_{pq}^{(2)})$ transform the electronic Hilbert space. For a \mathcal{D} -dimensional Hilbert space and $\theta \in \mathbb{R}$, the exponential operators $\exp(\theta \hat{\kappa}_I)$ belong to the $SO(\mathcal{D})$ matrix group and the anti-Hermitian operators $\hat{\kappa}_I$ belong to the associated Lie algebra $\mathfrak{so}(\mathcal{D})$.^(34, 35) Therefore, the operators $\exp(\theta \hat{\kappa}_{pq}^{(1)})$ and $\exp(\theta \hat{\kappa}_{pq}^{(2)})$ are isomorphic to rotations in Euclidean space. These rotations can be illustrated by considering the action of $\hat{\kappa}_{pq}^{(1)}$ and $\hat{\kappa}_{pq}^{(2)}$ on the singlet states for two

electrons in two spatial orbitals ϕ_p and ϕ_q , for which $\mathcal{D} = 3$. The complete $\mathfrak{so}(3)$ Lie algebra is then characterised by the commutation relations

$$[\hat{\kappa}_{pq}^{(1)}, \hat{\kappa}_{pq}^{(2)}] = 2\hat{\kappa}_{pq}^{(3)}, \quad [\hat{\kappa}_{pq}^{(2)}, \hat{\kappa}_{pq}^{(3)}] = 2\hat{\kappa}_{pq}^{(1)}, \quad [\hat{\kappa}_{pq}^{(3)}, \hat{\kappa}_{pq}^{(1)}] = 2\hat{\kappa}_{pq}^{(2)}, \quad (5)$$

where $\hat{\kappa}_{pq}^{(3)} \equiv 2[\hat{\kappa}_{pq}^{(1)}, \hat{\kappa}_{pq}^{(2)}]$ by definition. Matrix representations for these operators in the two-electron singlet basis $\{|q\bar{q}\rangle, \frac{1}{\sqrt{2}}(|q\bar{p}\rangle + |p\bar{q}\rangle), |p\bar{p}\rangle\}$, where e.g. $|q\bar{q}\rangle = \hat{q}^\dagger \hat{q}^\dagger |\text{vac}\rangle$, are given by

$$\hat{\kappa}_{pq}^{(1)} = \begin{pmatrix} 0 & -\sqrt{2} & 0 \\ \sqrt{2} & 0 & -\sqrt{2} \\ 0 & \sqrt{2} & 0 \end{pmatrix}, \quad \hat{\kappa}_{pq}^{(2)} = \begin{pmatrix} 0 & 0 & -2 \\ 0 & 0 & 0 \\ 2 & 0 & 0 \end{pmatrix}, \quad \text{and} \quad \hat{\kappa}_{pq}^{(3)} = \begin{pmatrix} 0 & \sqrt{2} & 0 \\ -\sqrt{2} & 0 & -\sqrt{2} \\ 0 & \sqrt{2} & 0 \end{pmatrix}. \quad (6)$$

Therefore, these operators are isomorphic to generators of rotations on the singlet hypersphere(36) (Fig. 1B) through e.g. $\hat{\kappa}_{pq}^{(1)} \cong \hat{L}_x$, $\hat{\kappa}_{pq}^{(2)} \cong \hat{L}_y$, and $\hat{\kappa}_{pq}^{(3)} \cong \hat{L}_z$. For many-electron systems, $\hat{\kappa}_{pq}^{(1)}$ and $\hat{\kappa}_{pq}^{(2)}$ mix determinants with the same electronic occupation excluding ϕ_p and ϕ_q , and form a universal set of Givens rotations,(37) as described in the supplementary discussion.

In 3D Euclidean space, any rotation \hat{R} of the axis system can be parametrised using three Euler angles $(\theta_1, \theta_2, \theta_3)$ and two distinct rotation axes (e.g. x and y) as(35)

$$\hat{R}(\theta_1, \theta_2, \theta_3) = \exp(\theta_1 \hat{L}_x) \exp(\theta_2 \hat{L}_y) \exp(\theta_3 \hat{L}_x). \quad (7)$$

Therefore, the singlet Hamiltonian for two-electrons in ϕ_p and ϕ_q can be completely diagonalised using the $\hat{U}_{pq}^{(m)}(\theta_1, \theta_2, \theta_3)$ operation proposed in Eq. (4), and we do not need to explicitly consider $\hat{\kappa}_{pq}^{(3)}$. In contrast, the operators $\hat{U}_{pq}^{\text{QNP}}(\theta_1, \theta_2) = \exp(\theta_1 \hat{\kappa}_{pq}^{(1)}) \exp(\theta_2 \hat{\kappa}_{pq}^{(2)})$ used in the QNP *ansatz*(27) cannot perform an arbitrary axis transformation in this 3-dimensional Hilbert space.(18, 19)

The ability of $\hat{U}_{pq}^{(m)}(\theta_1, \theta_2, \theta_3)$ to perform any transformation within the two-electron, two-orbital Hilbert space provides the tUPS *ansatz* with greater variational flexibility than the QNP gate fabric, particularly when the wave function is not dominated by a single determinant. Therefore, the tUPS *ansatz* will converge faster than the QNP approach with respect to the number of layers for deep quantum circuits and multi-configurational ground states. Furthermore, we can exploit the four-point parameter shift rule(38, 39) derived for the QNP gate fabric(27) to evaluate analytic partial derivatives with respect to the tUPS parameters, as detailed in the supplementary discussion.

Convergence to the exact ground state

Convergence to the exact ground state for $L \rightarrow \infty$ is guaranteed by the relationship of the tUPS *ansatz* to the general UPS structure [Eq. (1)] and stems from disentangling the fermionic Lie algebra.(18, 19) Since every many-body excitation can be expressed using nested commutators containing only operators of the form $\hat{\kappa}_{pq}^{(1)}$ and $\hat{\kappa}_{pq}^{(2)}$, the spin-adapted one-body and paired two-body operators can “generate” the full Lie algebra of many-body excitations.(18, 25) Expanding the product of exponential operators using the Baker–Campbell–Hausdorff theorem,(34) $e^{\hat{A}} e^{\hat{B}} = e^{\hat{A} + \hat{B} + \frac{1}{2}[\hat{A}, \hat{B}] + \dots}$, ensures that Eq. (1) can represent any fermionic unitary transformation for a sufficiently large L . This result extends to the tUPS approach by noting that any spin-adapted one-body or paired two-body operator can be represented in terms of a sum of operators and commutators that only include $\hat{\kappa}_{p,p\pm 1}^{(1)}$ or $\hat{\kappa}_{p,p\pm 1}^{(2)}$, as shown in the supplementary discussion.

Conserving quantum numbers such as the particle number, $\langle \hat{S}_z \rangle$, and $\langle \hat{S}^2 \rangle$ ensures that approximate wave functions can be physically interpreted and have a high overlap with the true ground

state, making them suitable initial states for fault-tolerant quantum algorithms.(1, 40) Employing fermionic operators means that truncated tUPS approximations conserve particle number and Pauli antisymmetry, which can be broken using gate-efficient qubit excitation operators.(15, 16, 24, 26, 41) The $\langle \hat{S}_z \rangle$ and $\langle \hat{S}^2 \rangle$ expectation values of $|\Phi_0\rangle$ are conserved because the spin-adapted one-body and paired two-body operators commute with the spin operators, e.g. $[\hat{S}_z, \hat{\kappa}_{pq}^{(1)}] = 0$ and $[\hat{S}^2, \hat{\kappa}_{pq}^{(1)}] = 0$. Furthermore, these operators can be implemented exactly as a quantum circuit, whereas spin-adapted unpaired two-body operators contain a sum of non-commuting terms that requires a Trotter approximation, which destroys the spin adaptation.(42)

Efficiency of quantum resources

In practice, the fermionic operators must be expressed as elementary qubit gates using transformations such as the Jordan–Wigner (JW) encoding(43) $\hat{p} = \frac{1}{2}(\hat{X}_p + i\hat{Y}_p) \prod_{r=0}^{p-1} \hat{Z}_r$, and $\hat{p}^\dagger = \frac{1}{2}(\hat{X}_p - i\hat{Y}_p) \prod_{r=0}^{p-1} \hat{Z}_r$. Here, $\{\hat{X}_p, \hat{Y}_p, \hat{Z}_p\}$ are the Pauli operators for the p^{th} qubit and $\prod_{r=0}^{p-1} \hat{Z}_r$ encodes the fermionic anti-symmetry. Since two-qubit CNOT gates create more noise than single-qubit gates, the CNOT count is commonly used to assess the practicality of a quantum circuit. For arbitrary many-body excitation operators, the CNOT count is dominated by the Pauli- Z string and increases with the number of orbitals.(44) This cost can be reduced by using the qubit creation and annihilation operators $\hat{Q}_p^\dagger = \frac{1}{2}(\hat{X}_p - i\hat{Y}_p)$ and $\hat{Q}_p = \frac{1}{2}(\hat{X}_p + i\hat{Y}_p)$ to define qubit-excitation-based (QEB) operators. (24, 26, 41, 44, 45) While one- and two-body QEB operators yield efficient circuit implementations,(44) and can be used in ADAPT-VQE,(24, 45) they ignore Pauli antisymmetry and can destroy the sign structure of the wave function.(26, 41)

The tUPS *ansatz* avoids any compromise between CNOT efficiency and symmetry preservation. If the spin-orbitals are indexed such that $\hat{\kappa}_{p,p\pm 1}^{(1)}$ acts between adjacent qubits, with the ordering

$$\{\phi_1, \phi_2, \dots, \phi_N, \phi_{\bar{N}}, \dots, \phi_{\bar{2}}, \phi_{\bar{1}}\}, \quad (8)$$

then the JW encoding of the spin-adapted one-body operator becomes equivalent to a QEB single excitation and the corresponding unitary operation becomes

$$\exp\left(\theta \hat{\kappa}_{p,p\pm 1}^{(1)}\right) = \exp\left(i\frac{\theta}{2}(\hat{X}_p \hat{Y}_{p\pm 1} - \hat{Y}_p \hat{X}_{p\pm 1})\right) \exp\left(i\frac{\theta}{2}(\hat{X}_{N+p} \hat{Y}_{N+p\pm 1} - \hat{Y}_{N+p} \hat{X}_{N+p\pm 1})\right), \quad (9)$$

where p and $p + N$ index the qubits representing the high- and low-spin orbitals for the spatial orbital ϕ_p . These operators can be implemented with 4 CNOT gates.(27, 44) Similarly, the Pauli- Z strings cancel for the paired two-body operators,(13, 25) allowing $\exp(\theta \hat{\kappa}_{p,p\pm 1}^{(2)})$ to be encoded with 13 CNOT gates.(27, 44) Circuit implementations for these operations are described in Ref. (27). Furthermore, $\hat{\kappa}_{p,p\pm 1}^{(2)}$ could be implemented with local qubit interactions using a 2D qubit arrangement that satisfies the order in Eq. (8) and provides local connectivity between the high- and low-spin states for spatial orbitals ϕ_p and $\phi_{p\pm 1}$, as suggested in Fig. 1C. Consequently, each $\hat{U}_{p,p\pm 1}^{(m)}$ operator can be implemented with 21 CNOT gates while conserving the particle number, $\langle \hat{S}^2 \rangle$ and $\langle \hat{S}_z \rangle$, and anti-symmetry of $|\Phi_0\rangle$, and the overall CNOT count for the tUPS *ansatz* is $21 L (N - 1)$.

Optimal orbitals and initial qubit state

Orbital optimisation has been shown to increase the accuracy of VQE for the UCC *ansatz* restricted to double excitations(10, 46–48) or separable pair approximations.(13) Crucially, these improvements do not increase the circuit depth since the orbital update can be classically implemented by transforming the input molecular integrals, while computing the orbital gradient requires at most

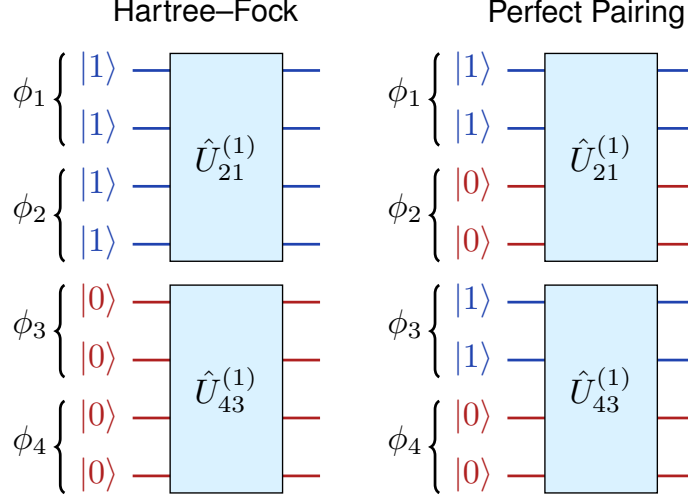


FIG. 2: Different initial qubit registers with the first “half” layer of the tUPS *ansatz* correspond to either the Hartree–Fock (left) or Perfect Pairing (right) approximations. For the Hartree–Fock case, the $\hat{U}_{pq}^{(1)}$ operators only act between occupied–occupied or virtual–virtual orbital pairs, and thus do not change the wave function.

the two-body density matrix, which is already measured for energy estimation.(46, 49) Therefore, we expect that orbital optimisation in the oo-tUPS *ansatz* will be essential to maximise the accuracy of shallow quantum circuits, and we describe its implementation in the supplementary methods.

Since the operators $\hat{U}_{p,p\pm 1}^{(m)}$ only act between sequential spatial orbitals, the entanglement generated by the first tUPS layer can be maximised by alternating the initial qubit register between occupied and empty spatial orbitals (Fig. 2), with no change to the circuit cost. The first “half” layer is then equivalent to the classical perfect pairing (PP) approximation(32, 50) as described in the supplementary discussion, leading to the pp-tUPS *ansatz*. Since PP is a form of valence bond theory,(51, 52) we expect that shallow pp-tUPS approximations with this alternating initial qubit register will be most accurate using localised bonding and anti-bonding orbital pairs, reflecting the local qubit interactions in the circuit. These local interactions have previously been exploited for quantum *ansätze* based on separable pair approximations.(13, 14) Furthermore, the relationship to PP theory suggests that the $L = 1$ truncation will perform well for weakly interacting pairs of strongly correlated electrons, while strong inter-pair correlation will require more layers.

Characterising the tUPS *ansatz* properties

We performed numerical VQE simulations to examine the accuracy of the tUPS *ansatz* structure, as detailed in the Methods section. The faster convergence with respect to the number of layers of the oo-tUPS and pp-tUPS approximations is demonstrated in the linear and triangular isomorphs of H_6 (STO-3G) with a nearest-neighbour separation of $R(H-H) = 2.0 \text{ \AA}$. For the linear structure, this bond length lies between the weakly correlated (equilibrium) and the strongly correlated (dissociation) regimes. The triangular structure corresponds to a spin-frustrated lattice, with no configuration where only opposite-spin electrons occur on neighbouring atoms.

First, we compare the tUPS accuracy with the original QNP approach(27) for a given L , noting that each QNP layer contains 10 operators and 85 CNOTs compared to 15 operators and 105 CNOTs for the tUPS *ansatz*. Using the ground-state Hartree–Fock (HF) orbitals for linear H_6 , the QNP approximation requires $L = 5$ to obtain chemical accuracy (1.59 mE_h), while the tUPS approach requires only $L = 4$ (Fig. 3A). The greater flexibility of the $\hat{U}_{pq}^{(m)}$ operators in the tUPS *ansatz* is essential when the wave function becomes increasingly entangled, providing lower energies

than QNP for deeper circuits. Including orbital optimisation significantly improves the accuracy for shallow circuits, deviating from the exact result by only $10^{-4} E_h$ for oo-tUPS with $L = 3$. Furthermore, the pp-tUPS approach requires only $L = 2$ to reach chemical accuracy, reducing the deviation in the energy by a factor of 10^3 compared to the HF-based tUPS *ansatz* with the same circuit depth. Consequently, our approach reduces the number of operators required to reach chemical accuracy in linear H_6 from 50 to 30 with the QNP and pp-tUPS methods, respectively, and the number of CNOT gates from 425 to 210.

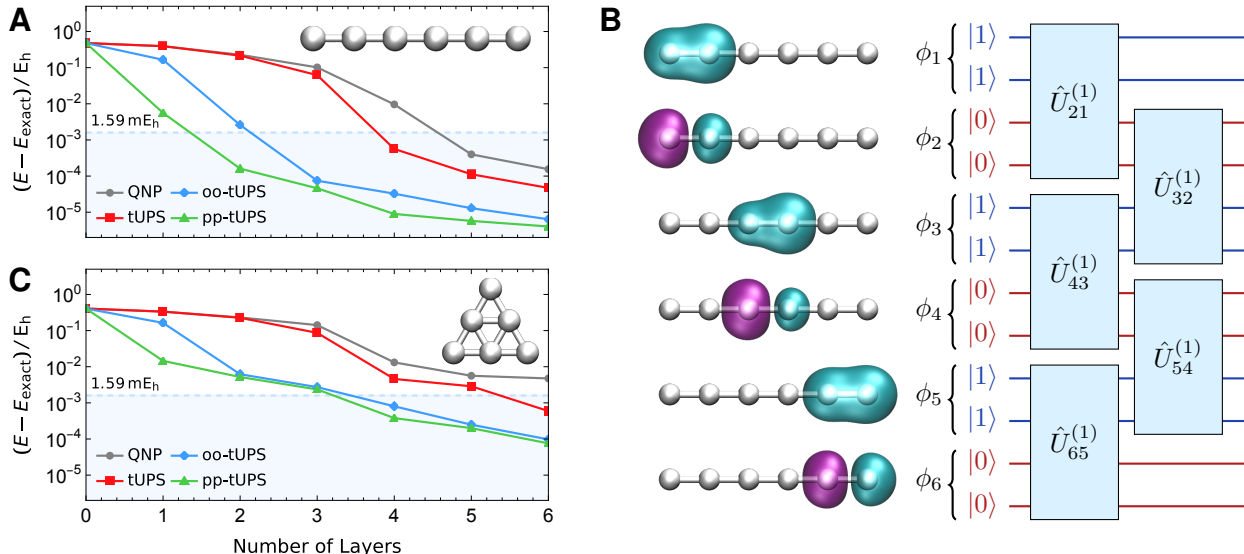


FIG. 3: The tUPS, oo-tUPS, and pp-tUPS methods accelerate the energy convergence with respect to the number of layers for (A) linear H_6 and (C) triangular H_6 with $R(\text{H-H}) = 2.0 \text{ \AA}$. (B) The optimal orbitals of the pp-tUPS *ansatz* ($L = 1$) for linear H_6 form localised bonding and anti-bonding orbital pairs, highlighting the importance of local interactions. Molecular geometries are provided in the supplementary methods.

While the wave function will be orbital-independent in the $L \rightarrow \infty$ limit, truncated approximations will depend on the choice of molecular orbitals. The optimal pp-tUPS orbitals for linear H_6 with $L = 1$ form pairs of localised bonding and anti-bonding orbitals between alternating bonds in the molecule (Fig. 3B). These optimal orbitals illustrate the close relationship between quantum approximations with local qubit connectivity and valence bond theory, providing physical intuition into how these quantum *ansätze* capture electron correlation. This pairing-based intuition suggests that the pp-tUPS approximation can provide chemically-accurate energies with $L = 2$ because the circuit structure can capture both intra- and inter-pair correlations for this system with three pairs of strongly interacting electrons.

The spin-frustrated triangular H_6 structure exhibits stronger electron correlation, with many near-degenerate configurations that provide a significant contribution to the ground state. The original QNP approach(27) fails to reach chemical accuracy within 6 layers (Fig. 3C). In contrast, the standard tUPS *ansatz* can achieve chemical accuracy with $L = 6$, demonstrating that the greater flexibility of $\hat{U}_{pq}^{(m)}$ defined in Eq. (4) is vital for strongly entangled states, where arbitrary unitary transformations are required. The oo-tUPS and pp-tUPS methods provide further improvement, with $L = 4$ sufficient to reach chemical accuracy in both cases. Although this system cannot be easily decomposed into weakly-interacting pairs of electrons, the pp-tUPS initial qubit state still improves the accuracy of shallow circuits compared to oo-tUPS by maximising the correlation captured by the first layer of the *ansatz*.

Achieving gate efficiency

The practicality of *ansatz* preparation on real quantum hardware is dominated the number of two-qubit CNOT gates, which provide the greatest contribution to the circuit noise. We investigated the accuracy and gate-efficiency of the tUPS approximation using the linear and triangular H_6 structures, the weakly correlated LiH molecule, and the delocalised π -system in benzene. We assume that spin-adapted one-body and paired two-body operators in the tUPS *ansatz* require 4 and 13 CNOT gates, respectively, using the circuit implementations described in Ref. (44).

For linear H_6 at $R(H-H) = 1.5 \text{ \AA}$, the fermionic-excitation-based(20) (FEB) or qubit-excitation-based(24) (QEB) variants of ADAPT-VQE require 1326 and 1410 CNOT gates to reach chemical accuracy, respectively, (Fig. 4A) while similar calculations using the selected projective quantum eigensolver (SPQE) converge with at least 4000 CNOT gates using the STO-6G basis set.(26, 41, 53) In contrast, only 568 CNOT gates are required if discrete optimisation is used to select the best operator sequence from a pool containing all spin-adapted one-body and paired two-body operators.(25) Remarkably, the pp-tUPS *ansatz* outperforms these adaptive methods and provides chemical accuracy with only 210 CNOT gates, giving an 84 % reduction relative to FEB-ADAPT-VQE. Orbital optimisation and the alternating initial qubit state are essential for achieving this gate efficiency, as demonstrated by comparing to the oo-tUPS and QNP approaches, which require 315 and 510 CNOT gates to reach chemical accuracy, respectively. Therefore, the pp-tUPS approach sets a new standard for the number of two-qubit CNOT gates required to obtain a chemically accurate quantum circuit for linear H_6 .

Since the triangular H_6 structure features stronger correlation than linear H_6 , adaptive methods

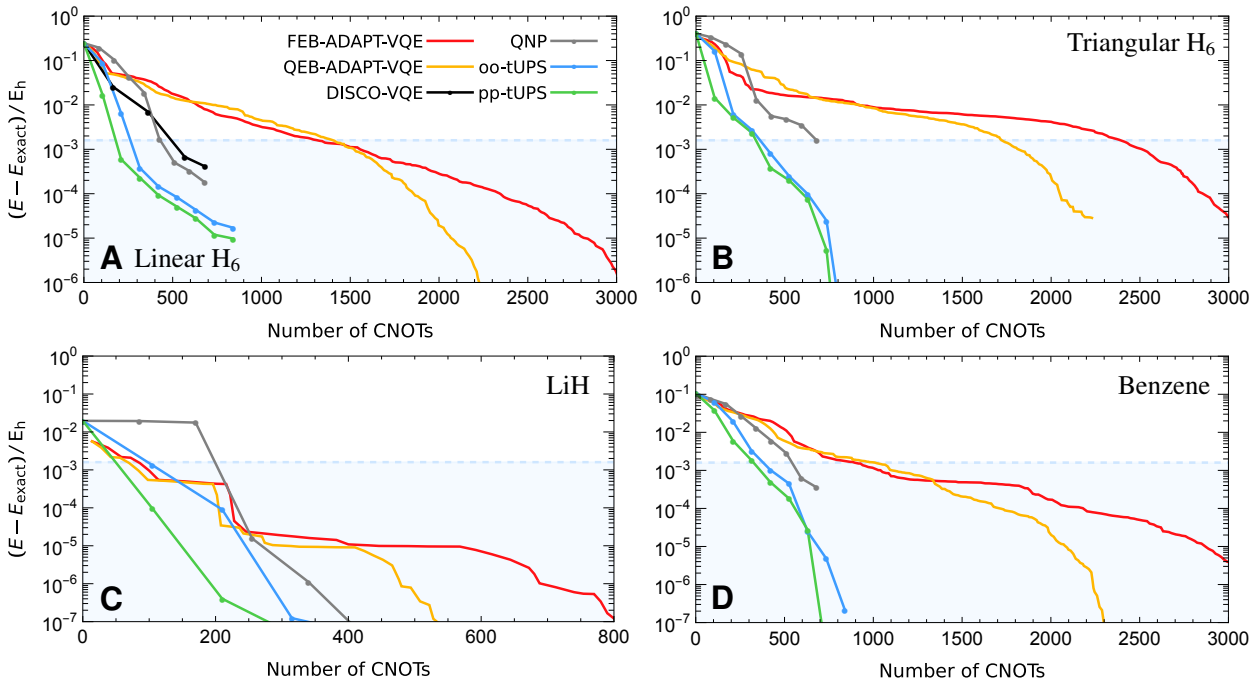


FIG. 4: The oo- and pp-tUPS methods significantly reduce the quantum resources required to quantitatively predict strongly correlated molecular energies compared to adaptive optimisation methods. The accuracy of the energy for a given number of CNOT gates is shown for (A) linear H_6 with $R(H-H) = 1.5 \text{ \AA}$, (B) triangular H_6 with $R(H-H) = 2.0 \text{ \AA}$, (C) LiH with $R(Li-H) = 1.546 \text{ \AA}$, and (D) benzene using the (6e, 6o) active space at the experimental geometry, provided in the supplementary methods. DISCO-VQE results are taken from Ref. (25) and are only available for linear H_6 .

such as ADAPT-VQE require more operators and CNOT gates to reach chemical accuracy, with 2402 and 1726 CNOT gates required for FEB-ADAPT-VQE and QEB-ADAPT-VQE, respectively (Fig. 4B). In contrast, the oo-tUPS and pp-tUPS approximations provide chemical accuracy with only 420 CNOT gates, giving an 82.5 % reduction compared to FEB-ADAPT-VQE. Therefore, the pp-tUPS *ansatz* can describe weak and strong correlation with a similar quantum resource cost.

The LiH and benzene molecules have been extensively studied using classical and quantum algorithms. At equilibrium, LiH is dominated by a single Slater determinant and both oo-tUPS and pp-tUPS provide chemical accuracy with $L = 1$, corresponding to 105 CNOT gates (Fig. 4C). Since LiH does not feature particularly strong correlation, the FEB- and QEB-ADAPT-VQE approaches provide similar gate efficiency to the pp-tUPS, although the pp-tUPS approximation converges more rapidly once the energy is within $10^{-4} E_h$ of the exact result. The pp-tUPS approach reaches chemical accuracy for benzene with 420 CNOT gates, compared to 896 for FEB-ADAPT-VQE, providing a reduction of 53 % (Fig. 4D). Consequently, the pp-tUPS approach significantly reduces the number of two-qubit CNOT gates required for chemically accurate predictions of both weakly and strongly correlated molecular energies, while also preserving the particle number, Pauli antisymmetry, $\langle \hat{S}_z \rangle$, and $\langle \hat{S}^2 \rangle$ symmetries of the initial state, and avoiding adaptive optimisation.

Predicting accurate potential energy surfaces

Chemical simulations rely on accurate predictions of molecular potential energy surfaces. However, classical methods struggle to balance the different correlation that occurs as molecular structures change, such as competing electronic configurations and spin-coupling during chemical reactions. We assessed the accuracy of tUPS, oo-tUPS, and pp-tUPS approximations for archetypal potential energy surfaces, including the dissociation of H₂O and N₂, and the insertion of Be into H₂.

Smooth potential energy surfaces are required to compute nuclear forces for geometry optimisation or dynamic simulations. Orbital optimisation in the oo-tUPS or pp-tUPS methods is essential to obtain smooth energy surfaces for all the molecules considered (Fig. 5). In contrast, the HF-based tUPS *ansatz* “jumps” between different solutions, despite using basin-hopping optimisation to identify the global minimum with respect to the continuous parameters. These jumps are worst for strongly correlated states, such as the molecular dissociation limit.

The accuracy of the oo-tUPS and pp-tUPS *ansatz* for dissociated H₂O and N₂ provides intuition into how electron correlation is captured. The symmetric stretch of H₂O simultaneously breaks two bonds into two spatially separated pairs of spin-coupled electrons. The pp-tUPS approximation accurately captures this correlation with $L = 1$ because the first half-layer strongly couples the electrons within each pair, and the second half-layer introduces the inter-pair coupling (Fig. 5A). In contrast, the oo-tUPS *ansatz* requires $L = 2$ to predict the correct dissociation limit since the HF-style initial qubit register is less efficient at describing the spin-coupled electron pairs. Similarly, breaking the N₂ triple bond gives three pairs of spin-coupled electrons and the pp-tUPS approximation requires $L = 2$ to capture the inter-pair correlation, while the oo-tUPS approach accurately predicts the dissociation limit with $L = 3$ (Fig. 5B). These results suggest that the pp-tUPS method can dissociate L bonds using $L - 1$ layers, providing valuable intuition into the chemical applicability of this quantum *ansatz*.

Reaching chemical accuracy across a full potential energy surface with a consistent and small number of unitary operators is particularly challenging for adaptive optimisation methods, which typically require more operators for intermediate bond lengths or the strongly correlated dissociation limit.^(20, 24, 26, 41) In contrast, discrete global optimisation of the operator sequence showed that accurate binding curves for H₂O and N₂ can be achieved with a constant number of operators.⁽²⁵⁾ Using the pp-tUPS *ansatz*, two layers (36 operators; 252 CNOTs) are sufficient to get a chemically accurate binding curve for H₂O, while three layers (45 operators; 315 CNOTs) are required for N₂.

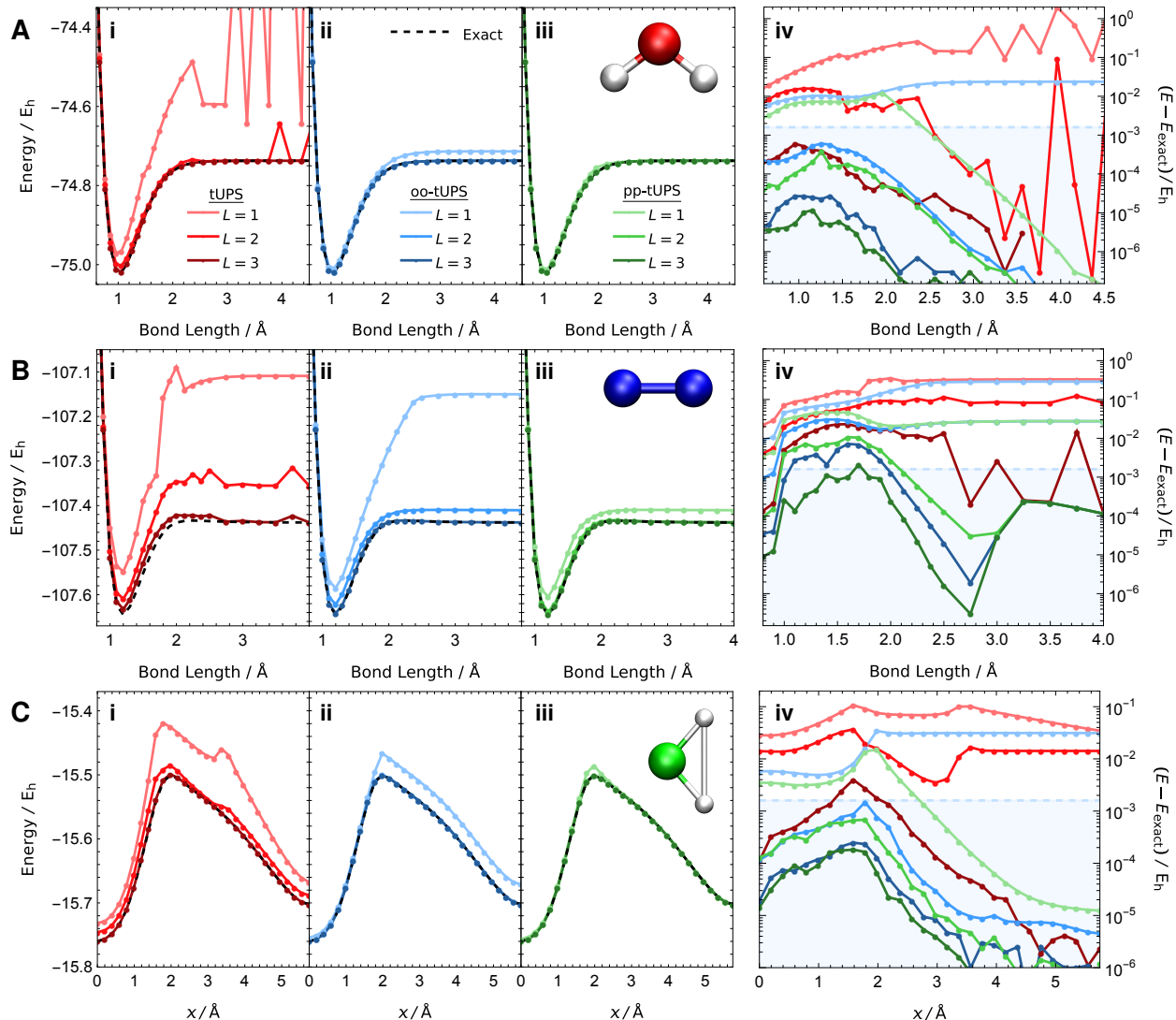


FIG. 5: Orbital optimisation is essential for computing smooth potential energy surfaces. Energy surfaces are computed for the H_2O (STO-3G) symmetric stretch (**A**), N_2 (STO-3G; 4 frozen core orbitals) dissociation (**B**), and $\text{Be} + \text{H}_2$ (STO-6G) insertion pathway (**C**) using the tUPS (**i**), oo-tUPS (**ii**), and pp-tUPS (**iii**) approximations, with the energetic accuracy compared in (**iv**). Molecular geometries are detailed in the supplementary methods.

By comparison, analogous FEB-ADAPT-VQE calculations required around 400 and 2000 CNOT gates to reach chemical accuracy for equilibrium and stretched N_2 , respectively.⁽²³⁾ The ability of pp-tUPS to give chemical accuracy for different geometries with a consistent number of CNOT gates will be essential for balancing the quantum hardware noise along potential energy surfaces.

Compared to the spin-coupling correlation for bond dissociation, the $\text{Be} + \text{H}_2$ insertion mechanism features strong mixing between two dominant closed-shell configurations.⁽⁵⁴⁾ We consider the reaction trajectory defined in Ref. ⁽⁵⁵⁾ with the STO-6G basis used in Ref. ⁽²⁶⁾. Like the H_2O and N_2 binding curves, orbital optimisation is essential to obtain a smooth potential energy surface (Fig. 5C). However, one layer of the oo-tUPS *ansatz* is not sufficient to get a balanced binding curve, giving less accurate energies for the dissociated regime where there is competition between the Be

$(1s)^2(2s)^2$ and $(1s)^2(2p)^2$ configurations(56) (Fig. 5C). The pp-tUPS *ansatz* provides qualitative accuracy with $L = 1$ (18 operators; 126 CNOTs) and reaches chemical accuracy at all points with $L = 2$ (36 operators; 252 CNOTs). The highly-accurate dissociation limit of pp-tUPS with $L = 1$ can be rationalised as there are two correlated pairs of electrons on the Be atom, and the overall system is a direct product of the Be and H_2 wave functions. Crucially, the pp-tUPS *ansatz* achieves this accuracy with a consistent wave function structure, while adaptive techniques typically select between $\times 5$ to $\times 130$ more operators at the crossing point ($x \sim 2 \text{ \AA}$) compared to the dissociation limit.(26)

Computing spin-state energetics

Resolving the energies of different spin states, such as as singlet-triplet gaps, is important for developing efficient organic light-emitting diodes, singlet fission, and photocatalysis. However, current quantum algorithms can only compute spin energetics using excited-state methods such as variational quantum deflation,(57) constraining $\langle \hat{S}^2 \rangle$ using Lagrange multipliers,(58) or subspace expansions such as the nonorthogonal VQE(59) and quantum equation-of-motion methods.(60–64) Since the tUPS *ansatz* only contains operators that commute with \hat{S}_z and \hat{S}^2 , the spin of the initial state is conserved for all truncations. Therefore, different spin-state energies can now be computed on an equal footing using suitable initial states, without any modifications to the VQE optimisation.

We first illustrate this approach using the bending mode of methylene, which involves a crossing of the S_0 and T_0 states. Both the oo-tUPS and pp-tUPS approximations qualitatively reproduce the singlet-triplet intersection point with $L = 2$ (36 operators; 252 CNOTs) and can predict the singlet-triplet gap $\Delta E_{ST} = E_S - E_T$ to within chemical accuracy at all points with $L = 3$ (54 operators; 378 CNOTs), as shown in Fig. 6. Like the ground-state potential energy surfaces, the pp-tUPS is more accurate than oo-tUPS for $L = 1$. However, this improvement is less significant for the T_0 state since the pp-tUPS *ansatz* cannot capture any additional correlation between the triplet-coupled electrons.

Tetramethylethane (TME) is a more challenging disjoint diradical, where the degenerate molecular orbitals are spatially separated.(65, 66) The $(6e, 6o)$ active space corresponding to the carbon π -system provides the natural approximation for predicting ΔE_{ST} . Both the oo-tUPS and

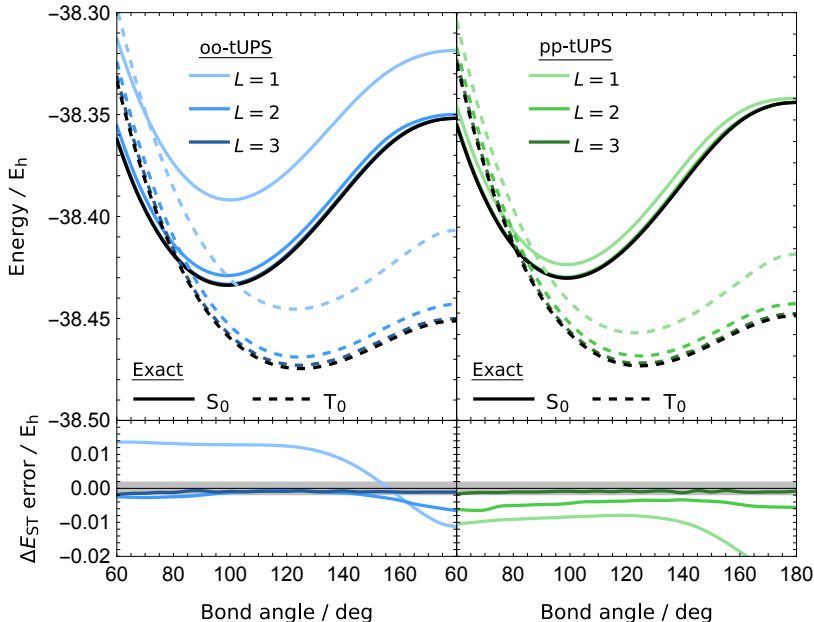


FIG. 6: The oo-tUPS and pp-tUPS *ansätze* accurately predict the singlet-triplet gap of methylene (STO-3G) with $R(C-H) = 1.117 \text{ \AA}$ by preserving the $\langle \hat{S}_z \rangle$ and $\langle \hat{S}^2 \rangle$ quantum numbers of the initial state.

pp-tUPS approaches systematically converge to the exact S_0 and T_0 energies as the number of *ansatz* layers is increased (Fig. 7). The pp-tUPS approach provides a balanced representation of the two states and can predict the singlet-triplet energy gap within chemical accuracy using two-layers (30 operators; 210 CNOTs). Again, the oo-tUPS approximation is less accurate for shallow circuits, but quantitatively predicts the singlet-triplet gap with $L = 3$. Consequently, the tUPS *ansatz* allows different spin states to be directly targeted in the VQE formalism, which was previously challenging using non-symmetry-preserving adaptive optimisation techniques.

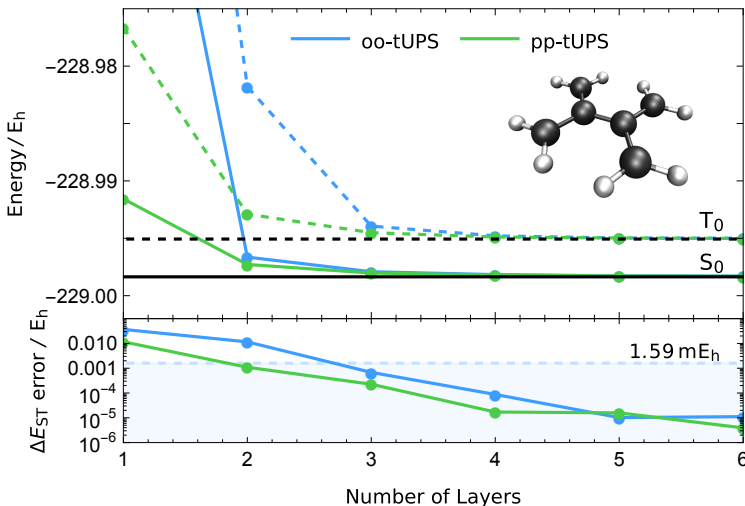


FIG. 7: The oo-tUPS and pp-tUPS *ansätze* systematically converge to the exact S_0 and T_0 energies for planar TME as more layers are added to the *ansatz*. The π -system (6e, 6o) active space is used with the STO-3G basis set at the molecular geometry provided in the supplementary methods. The singlet-triplet gap (ΔE_{ST}) can be predicted within chemical accuracy using two layers (30 operators; 210 CNOTs) of the pp-tUPS *ansatz*.

Discussion

We have shown that physically-accurate parametrisations for electronic states can be constructed with very shallow quantum circuits using the fixed pp-tUPS *ansatz*, avoiding expensive adaptive optimisation methods. This *ansatz* is systematically improvable, and combines physical accuracy with gate efficiency while conserving particle number, fermionic antisymmetry, and the $\langle \hat{S}_z \rangle$ and $\langle \hat{S}^2 \rangle$ quantum numbers of the initial state. The accuracy that can be achieved with shallow quantum circuits is maximised by incorporating orbital optimisation and an initial qubit register that is derived from perfect pairing valence bond theory. Numerical simulations on molecules with strongly correlated electronic states demonstrate that chemically accurate potential energy surfaces and singlet-triplet gaps can be predicted with significantly fewer two-qubit CNOT gates compared to state-of-the-art adaptive optimisation methods.

Previously, adaptive optimisation has been essential to identify a physically accurate sequence of unitary operators with shallow quantum circuit implementations.^(20, 24, 25) In contrast, the pp-tUPS *ansatz* achieves accuracy and gate efficiency by using fermionic operators that only act between nearest-neighbour spatial orbitals and by considering their properties as Lie algebraic generators for unitary transformations. This paradigm shift away from adaptive *ansatz* design offers key advantages for practical quantum simulations: it avoids the measurement costs required to adaptively optimise the operator sequence; and gives a consistent circuit structure with a well-defined quantum resource cost across all molecular structures. These advances lay the foundation

for a new generation of high-accuracy fixed approximations for electronic states that embrace the natural functionality of qubit rotations, without sacrificing fundamental physical symmetries.

This work has considered the full expressibility of the tUPS *ansatz* hierarchy using global optimisation techniques. Future investigations will be required to understand the numerical optimisation of the energy, including the best optimisation algorithm, and the structure of the underlying energy landscape. While connections to valence bond theory will guide the identification of suitable initial guesses, it is not clear whether the *ansatz* structure, or the inclusion of orbital optimisation, will improve or worsen the issues of local minima and barren plateaus in variational quantum algorithms.(67, 68) Further numerical simulations will be necessary to assess how much the reduction in CNOT gates improves the noise resilience of the corresponding quantum circuits, whether the accuracy remains consistent for larger systems, and how many circuit layers are needed.

Preparing physically accurate and gate-efficient quantum representations of electronic states will be vital to capitalise on the functionality of near-term quantum computing. Current state-of-the-art methods adaptively design the *ansatz* for each molecule, but these have high quantum measurement costs, give different circuits along potential energy surfaces, and struggle to preserve spin symmetry. We have presented the pp-tUPS *ansatz*, which achieves both gate-efficiency and symmetry preservation using a fixed circuit structure, and can achieve chemical accuracy for strongly correlated molecules using as much as 84 % fewer two-qubit gates compared to adaptive techniques. We believe that this *ansatz* will pave the way for practical electronic structure simulations of strongly correlated chemistry on real quantum hardware.

Methods

Numerical tUPS simulations

All molecular energies were computed using state-vector VQE simulations following the protocol described in supplementary section “*Continuous optimisation using basin-hopping*” of Ref. (25), as summarised here. Molecular one- and two-electron integrals were computed using PYSCF(69) for the molecular structures and active orbital spaces detailed in the supplementary methods. Matrix representations of the Hamiltonian and the fermionic $\hat{\kappa}_{pq}^{(1)}$ and $\hat{\kappa}_{pq}^{(2)}$ operators were generated in the number-preserving and $\langle S_z \rangle = 0$ Hilbert space using OPENFERMION.(70) VQE calculations were then simulated using a developmental version of the GMIN global optimisation program.(71) The continuous *ansatz* parameters were optimised using analytic gradients and a customised version of the L-BFGS algorithm,(72–76) as implemented in GMIN. Basin-hopping parallel tempering(77–79) was employed to efficiently search the continuous energy landscape, which can be highly non-convex. The optimisation parameters for each molecule are summarised in supplementary table 1.

While orbital optimisation can be implemented by transforming the molecular integrals used in the VQE simulation, the structure of our computational workflow required a different approach. We implemented orbital optimisation by applying a series of one-body operators after the tUPS *ansatz* structure (i.e., at the end of the state preparation circuit) and including the orbital rotation angles as additional parameters in the VQE optimisation. This series of one-body operators was constructed using a tiled circuit structure containing $\frac{1}{2}N(N-1)$ rotation angles, which corresponds to the dimensionality of the orbital rotation space, as described in the supplementary methods. The alternating initial qubit state was prepared by applying a suitable series of paired two-body operators to the HF ground state. For triplet calculations, the initial state was prepared by applying the triplet excitation operator(28) $\hat{T}_{pq} = \frac{1}{\sqrt{2}}(\hat{p}^\dagger \hat{q} - \hat{p} \hat{q}^\dagger)$ to the doubly-occupied HOMO-LUMO orbital pair. Since triplet calculations were always performed with orbital optimisation, the initial orbitals were not adjusted prior to the VQE optimisation.

FEB- and QEB-ADAPT-VQE simulations

Fermionic-excitation-based (FEB) and qubit-excitation-based (QEB) ADAPT-VQE simulations were performed with the QFORTE program.⁽⁸⁰⁾ The operator pool contained all generalised one- and two-body fermionic or qubit excitation operators without any spin adaption. Calculations were performed up to a maximum of 200 operators and the corresponding number of CNOT gates was computed using the circuit implementations provided in Ref. (24).

References

- [1] S. McArdle, S. Endo, A. Aspuru-Guzik, S. C. Benjamin, X. Yuan, Quantum computational chemistry, *Reviews of Modern Physics* **92**, 15003 (2020).
- [2] A. Peruzzo, *et al.*, A variational eigenvalues solver on a photonic quantum processor, *Nat. Comm.* **5**, 4213 (2014).
- [3] A. Anand, *et al.*, A quantum computing view on unitary coupled cluster theory, *Chem. Soc. Rev.* **51**, 1659 (2022).
- [4] J. Tilly, *et al.*, The Variational Quantum Eigensolver: A review of methods and best practices, *Phys. Rep.* **986**, 1 (2022).
- [5] A. Kandala, *et al.*, Hardware-efficient variational quantum eigensolver for small molecules and quantum magnets, *Nature* **549**, 242 (2017).
- [6] I. G. Ryabinkin, S. N. Genin, A. F. Izmaylov, Relation between fermionic and qubit mean fields in the electronic structure problem, *J. Chem. Phys.* **149**, 214105 (2018).
- [7] R. D’Cunha, T. D. Crawford, M. Motta, J. E. Rice, Challenges in the Use of Quantum Computing Hardware-Efficient Ansätze in Electronic Structure Theory, *J. Phys. Chem. A* **127**, 3437 (2023).
- [8] M. Cerezo, A. Sone, T. Volkoff, L. Cincio, P. J. Coles, Cost function dependent barren plateaus in shallow parametrized quantum circuits, *Nat. Comm.* **12**, 1791 (2021).
- [9] J. Lee, W. J. Huggins, M. Head-Gordon, K. B. Whaley, Generalized Unitary Coupled Cluster Wave functions for Quantum Computation, *J. Chem. Theory Comput.* **15**, 311 (2019).
- [10] I. O. Sokolov, *et al.*, Quantum orbital-optimized unitary coupled cluster methods in the strongly correlated regime: Can quantum algorithms outperform their classical equivalents?, *J. Chem. Phys.* **152**, 124107 (2020).
- [11] M.-A. Filip, A. J. W. Thom, A stochastic approach to unitary coupled cluster, *J. Chem. Phys.* **153**, 214106 (2020).
- [12] Y. Matsuzawa, Y. Kurashige, Jastrow-type Decomposition in Quantum Chemistry for Low-Depth Quantum Circuits, *J. Chem. Theory Comput.* **16**, 944 (2020).
- [13] J. S. Kottmann, A. Aspuru-Guzik, Optimized low-depth quantum circuits for molecular electronic structure using a separable-pair approximation, *Phys. Rev. A* **105**, 032449 (2022).
- [14] J. S. Kottmann, Molecular Quantum Circuit Design: A Graph-Based Approach, *Quantum* **7**, 1073 (2023).
- [15] I. G. Ryabinkin, T.-C. Yen, S. N. Genin, A. F. Izmaylov, Qubit Coupled Cluster Method: A Systematic Approach to Quantum Chemistry on a Quantum Computer, *J. Chem. Theory Comput.* **14**, 6317 (2018).
- [16] R. Xia, S. Kais, Qubit coupled cluster singles and doubles variational quantum eigensolver ansatz for electronic structure calculations, *Quantum Sci. Technol.* **6**, 015001 (2021).
- [17] H. R. Grimsley, D. Claudino, S. E. Economou, E. Barnes, N. J. Mayhall, Is the Trotterized UCCSD Ansatz Chemically Well-Defined?, *J. Chem. Theory Comput.* **16**, 1 (2020).
- [18] F. A. Evangelista, G. K.-L. Chan, G. E. Scuseria, Exact parameterization of fermionic functions via unitary coupled cluster theory, *J. Chem. Phys.* **151**, 244122 (2019).

- [19] A. F. Izmaylov, M. Díaz-Tinoco, R. A. Lang, On the order problem in the construction of unitary operators for the variational quantum eigensolver, *Phys. Chem. Chem. Phys.* **22**, 12980 (2020).
- [20] H. R. Grimsley, S. E. Economou, E. Barnes, N. J. Mayhall, An adaptive variational algorithm for exact molecular simulations on a quantum computer, *Nat. Comm.* **10**, 3007 (2019).
- [21] H. L. Tang, *et al.*, Qubit-ADAPT-VQE: An Adaptive Algorithm for Constructing Hardware-Efficient Ansätze on a Quantum Processor, *PRX Quantum* **2**, 020310 (2021).
- [22] H. H. S. Chan, N. Fitzpatrick, J. Segarra-Martí, M. J. Bearpark, D. P. Tew, Molecular excited state calculations with adaptive wavefunctions on a quantum eigensolver emulation: reducing circuit depth and separating spin states, *Phys. Chem. Chem. Phys.* **23**, 26438 (2021).
- [23] T. Tsuchimochi, M. Taii, T. Nishimaki, S. L. Ten-no, Adaptive construction of shallower quantum circuits with quantum spin projection for fermionic systems, *Phys. Rev. Research* **4**, 033100 (2022).
- [24] Y. S. Yordanov, V. Armaos, C. H. W. Barnes, D. R. M. Arvidsson-Shukur, Qubit-excitation-based adaptive variational quantum eigensolver, *Commun. Phys.* **4**, 228 (2021).
- [25] H. G. A. Burton, D. Marti-Dafcik, D. P. Tew, D. J. Wales, Exact electronic states with shallow quantum circuits from global optimisation, *npj Quantum Inf.* **9**, 75 (2023).
- [26] I. Magoulas, F. A. Evangelista, CNOT-Efficient Circuits for Arbitrary Rank Many-Body Fermionic and Qubit Excitations, *J. Chem. Theory Comput.* **19**, 822 (2023).
- [27] G.-L. R. Anselmetti, D. Wierichs, C. Gogolin, R. M. Parrish, Local, expressive, quantum-number-preserving VQE ansätze for fermionic systems, *New J. Phys.* **23**, 113010 (2021).
- [28] T. Helgaker, P. Jørgensen, J. Olsen, *Molecular Electronic-Structure Theory* (John Wiley & Sons, 2000).
- [29] K. V. Lawler, D. W. Small, M. Head-Gordon, Orbitals That Are Unrestricted in Active Pairs for Generalized Valence Bond Coupled Cluster Methods, *J. Phys. Chem. A* **114**, 2930 (2010).
- [30] G. J. O. Beran, B. Austin, A. Sodt, M. Head-Gordon, Unrestricted Perfect Pairing: The Simplest Wave-Function-Based Model Chemistry beyond Mean Field, *J. Phys. Chem. A* **109**, 9183 (2005).
- [31] T. Van Voorhis, M. Head-Gordon, A nonorthogonal approach to perfect pairing, *J. Chem. Phys.* **112**, 5633 (2000).
- [32] A. C. Hurley, J. E. Lennard-Jones, J. A. Pople, The molecular orbital theory of chemical valency XVI. A theory of paired-electrons in polyatomic molecules, *Proc. Royal Soc. A* **220**, 446 (1953).
- [33] S. Lehtola, J. Parkhill, M. Head-Gordon, Orbital optimisation in the perfect pairing hierarchy: applications to full-valence calculations on linear polyacenes, *Mol. Phys.* **116**, 547 (2018).
- [34] B. C. Hall, *Lie Groups, Lie Algebras, and Representations* (Springer Chem, 2015).
- [35] R. Gilmore, *Lie Groups, Physics, and Geometry: An Introduction for Physicists, Engineers, and Chemists* (Dover Publications Inc., 2008), first edn.
- [36] H. G. A. Burton, Energy Landscape of State-Specific Electronic Structure Theory, *J. Chem. Theory Comput.* **18**, 1512 (2022).
- [37] J. M. Arrazola, *et al.*, Universal quantum circuits for quantum chemistry, *Quantum* **6**, 742 (2022).
- [38] K. Mitarai, M. Negoro, M. Kitagawa, K. Fujii, Quantum circuit learning, *Phys. Rev. A* **98**, 032309 (2018).
- [39] D. Wierichs, J. Izaac, C. Wang, C. Y.-Y. Lin, General parameter-shift rules for quantum gradients, *Quantum* **6**, 677 (2022).
- [40] S. Lee, *et al.*, Evaluating the evidence of exponential quantum advantage in ground-state quantum chemistry, *Nat. Comm.* **14**, 1952 (2023).
- [41] I. Magoulas, F. A. Evangelista, Linear-Scaling Quantum Circuits for Computational Chemistry, *J. Chem. Theory Comput.* **19**, 4815 (2023).
- [42] T. Tsuchimochi, Y. Mori, S. L. Ten-no, Spin-projection for quantum computation: A low-depth approach to strong correlation, *Phys. Rev. Research* **2**, 043142 (2020).

- [43] P. Jordan, E. Wigner, Über das Paulische Äquivalenzverbot, *Z. Phys.* **47**, 631 (1928).
- [44] Y. S. Yordanov, D. R. M. Arvidsson-Shukur, C. H. W. Barnes, Efficient quantum circuits for quantum computational chemistry, *Phys. Rev. A* **102**, 062612 (2020).
- [45] Y. S. Yordanov, C. H. W. Barnes, D. R. M. Arvidsson-Shukur, Molecular-excited-state calculations with the qubit-excitation-based adaptive variational quantum eigensolver protocol, *Phys. Rev. A* **106**, 032434 (2022).
- [46] W. Mizukami, *et al.*, Orbital optimized unitary coupled cluster theory for quantum computer, *Phys. Rev. Research* **2**, 033421 (2020).
- [47] J. Bierman, Y. Li, J. Lu, Improving the accuracy of variational quantum eigensolvers with fewer qubits using orbital optimisation, *J. Chem. Theory Comput.* **19**, 790 (2023).
- [48] L. Zhao, *et al.*, Orbital-optimized pair-correlated electron simulations on trapped-ion quantum computers, *npj Quantum Inf.* **9**, 60 (2023).
- [49] T. Takeshita, *et al.*, Increasing the representation accuracy of quantum simulations of chemistry without extra quantum resources, *PRX* **10**, 011004 (2021).
- [50] W. J. Hunt, P. J. Hay, W. A. Goddard III, Self-Consistent Procedures for Generalized Valence Bond Wavefunctions. Applications H₃, BH, H₂O, C₂H₆, and O₂, *J. Chem. Phys.* **57**, 738 (1972).
- [51] J. Gerratt, D. L. Cooper, P. B. Karadakov, M. Raimondi, Modern valence bond theory, *Chem. Soc. Rev.* **26**, 87 (1997).
- [52] T. H. Dunning Jr., L. T. Xu, D. L. Cooper, P. B. Karadakov, Spin-Coupled Generalized Valence Bond Theory: New Perspectives on the Electronic Structure of Molecules and Chemical Bonds, *J. Phys. Chem. A* **125**, 2021 (2021).
- [53] N. H. Stair, F. A. Evangelista, Simulating Many-Body Systems with a Projective Quantum Eigensolver, *PRX Quantum* **2**, 030301 (2021).
- [54] G. D. Purvis III, R. J. Bartlett, A full coupled-cluster singles and doubles model: The inclusion of disconnected triples, *J. Chem. Phys.* **76**, 1910 (1982).
- [55] F. A. Evangelista, Alternative single-reference coupled cluster approaches for multireference problems: The simpler the better, *J. Chem. Phys.* **134**, 224102 (2011).
- [56] D. K. W. Mok, R. Neumann, N. C. Handy, Dynamical and Nondynamical Correlation, *J. Phys. Chem.* **100**, 6225 (1996).
- [57] Y. Ibe, *et al.*, Calculating transition amplitudes by variational quantum deflation, *Phys. Rev. Research* **4**, 013173 (2022).
- [58] S. Shirai, *et al.*, Computational Analysis of Chemical Reactions Using a Variational Quantum Eigensolver Algorithm without Specifying Spin Multiplicity, *ACS Omega* **8**, 19917 (2023).
- [59] U. Baek, *et al.*, Say NO to Optimization: A Nonorthogonal Quantum Eigensolver, *PRX Quantum* **4**, 030307 (2023).
- [60] A. Asthana, *et al.*, Quantum self-consistent equation-of-motion method for computing molecular excitation energies, ionization potentials, and electron affinities on a quantum computer, *Chem. Sci.* **14**, 2405 (2023).
- [61] J. Colless, *et al.*, Computation of Molecular Spectra on a Quantum Processor with an Error-Resilient Algorithm, *Phys. Rev. X* **8**, 011021 (2018).
- [62] P. J. Ollitrault, *et al.*, Quantum equation of motion for computing molecular excitation energies on a noisy quantum processor, *Phys. Rev. Research* **2**, 043140 (2020).
- [63] M. Matoušek, K. Pernal, F. Pavošević, L. Veis, Variational quantum eigensolver boosted by adiabatic connection arxiv:2310.05906 (2023).
- [64] Q. Gao, *et al.*, Applications of quantum computing for investigations of electronic transitions in phenylsulfonyl-carbazole TADF emitters, *npj Comput. Mater.* **7**, 70 (2021).

- [65] Z. D. Pozun, X. Su, K. D. Jordan, Establishing the Ground State of the Disjoint Diradical Tetramethyleneethane with Quantum Monte Carlo, *J. Am. Chem. Soc.* **135**, 12862 (2013).
- [66] L. Veis, A. Antalík, Örs Legeza, A. Alavi, J. Pittner, The Intricate Case of Tetramethyleneethane: A Full Configuration Interaction Quantum Monte Carlo Benchmark and Multireference Coupled Cluster Studies, *J. Chem. Theory Comput.* **14**, 2439 (2018).
- [67] L. Bittel, M. Kliesch, Training Variational Quantum Algorithms Is NP-Hard, *Phys. Rev. Lett.* **127**, 120502 (2021).
- [68] J. R. McClean, S. Boixo, V. N. Smelyanskiy, R. Babbush, H. Neven, Barren plateaus in quantum neural network training landscapes, *Nat. Comm.* **9**, 4812 (2018).
- [69] Q. Sun, *et al.*, Recent developments in the PySCF program package, *J. Chem. Phys.* **153**, 024109 (2020).
- [70] J. R. McClean, *et al.*, OpenFermion: the electronic structure package for quantum computers, *Quantum Sci. Technol.* **5**, 034014 (2020).
- [71] GMIN: A program for finding global minima and calculating thermodynamic properties, <http://www-wales.ch.cam.ac.uk/software.html>.
- [72] J. Nocedal, Updating quasi-Newton matrices with limited storage, *Math. Comp.* **35**, 773 (1980).
- [73] C. G. Broyden, The Convergence of a Class of Double-rank Minimization Algorithms 1. General Considerations, *IMA J. Appl. Math.* **6**, 76 (1970).
- [74] R. Fletcher, A new approach to variable metric algorithms, *Comput. J.* **13**, 317 (1970).
- [75] D. Goldfarb, A family of variable-metric methods derived by variational means, *Math. Comp.* **24**, 23 (1970).
- [76] D. F. Shanno, Conditioning of quasi-Newton methods for function minimization, *Math. Comp.* **24**, 647 (1970).
- [77] Z. Li, H. A. Scheraga, Monte carlo-minimization approach to the multiple-minima problem in protein folding, *PNAS* **84**, 6611 (1987).
- [78] D. J. Wales, J. P. K. Doye, Global Optimization by Basin-Hopping and the Lowest Energy Structures of Lennard-Jones Clusters Containing up to 110 Atoms, *J. Phys. Chem. A* **101**, 5111 (1997).
- [79] B. Strodel, J. W. L. Lee, C. S. Whittleston, D. J. Wales, Transmembrane structures for alzheimer's $\alpha\beta 1-42$ oligomers, *J. Am. Chem. Soc.* **132**, 13300 (2010).
- [80] N. H. Stair, F. A. Evangelista, QFort: An Efficient State-Vector Emulator and Quantum Algorithms Library for Molecular Electronic Structure, *J. Chem. Theory Comput.* **18**, 1555 (2022).

Acknowledgements

The author acknowledges insightful discussions with Daniel Marti-Dafcik, David Tew, Paul Johnson, Alex Thom, and Pierre-François Loos. HGAB was supported by Downing College, Cambridge through the Kim and Julianna Silverman Research Fellowship.

Author contributions:

HGAB conceived the project, performed the theoretical and numerical analysis, and wrote the manuscript.

Competing interests:

The author declares that they have no competing interests.

Data availability:

The numerical data required to reproduce all figures will be made available online in an open-access repository after publication.

Code availability:

The code for the numerical simulations is available upon reasonable request.